# ARTIFICIAL INTELLIGENCE-BASED FAULT DETECTION IN PHOTOVOLTAIC POWER PLANTS USING DRONE-ACQUIRED THERMAL IMAGING

**Eduardo Martins da Silva[1], Daniel Henrique Nogueira Dias[1], Vitor Hugo Ferreira[1], Gilberto Figueiredo Pinto Filho[1] and Wanderson da Silva Corrêa[1].**

[1] Universidade Federal Fluminense, Niterói - RJ - Brazil

**Abstract**

This work presents an intelligent technique to support maintenance in large-scale photovoltaic power plants, utilizing a semi-automated pipeline that combines manual data acquisition with automated AI-powered analysis. The solution was designed and validated to streamline the monitoring procedure at the Fluminense Federal University (UFF) photovoltaic plant in Prédio H - Praia Vermelha Campus. A certified pilot operates a DJI Matrice 30 Thermal (M30T) drone to manually conduct flights and collect thermal images of the solar panels. After data transfer, an AI algorithm, based on the YOLOv8 architecture, automatically analyzes the thermal images to detect and classify anomalies, with a primary focus on hotspots. The trained model achieved a robust performance in hotspot detection, reaching a mean Average Precision (mAP@0.5) of 85.3%. This automated classification process significantly accelerates Operation and Maintenance (O&M) workflows, making the application a commercially viable tool for predictive maintenance in the PV industry. The final system issues alerts indicating the exact position (X, Y coordinates) and ID of the faulty panel, enabling targeted and efficient repair interventions.

*Keywords: Large scale photovoltaic systems, predictive maintenance, Artificial Intelligence, fault detection, Thermography, YOLOv8, O&M.*

## 1. Introduction

The increase of large-scale photovoltaic (PV) systems worldwide demands efficient and precise maintenance strategies to ensure optimal energy production and equipment longevity (Abubakar, A. et al, 2021). Traditional inspection methods, often manual and time-consuming, are increasingly inadequate for the vast scale of modern solar plants (Madeti, S.R. et al 2017 and Tsanakas, J.A. et al, 2020). In response, the integration of autonomous drones equipped with thermal imaging and advanced artificial intelligence (AI) algorithms has emerged as a transformative solution for PV plant maintenance (Redondo, E. et al, 2022). This study presents the development and implementation of an intelligent software system designed to automate the post-flight analysis stage of PV plant maintenance. The system was deployed and validated at the Fluminense Federal University's solar power plant in Prédio H - Praia Vermelha Campus, Rio de Janeiro, Brazil. It utilizes a DJI Matrice 30 Thermal drone, operated by a pilot, to conduct systematic flights and capture high-resolution thermal images. By automating the analysis of these images using a state-of-theart AI model, the system drastically reduces inspection time and enhances the efficiency of maintenance interventions. When a fault, such as a hotspot, is identified, the system generates a precise alert specifying the panel's location, facilitating targeted repairs. When a fault is identified, the system generates an alert specifying the panel's position (X, Y) and unique ID, facilitating targeted maintenance interventions. The implementation of this system aligns with international standards for drone-based PV inspections, such as IEC 62446-3:2017, which emphasizes the importance of high-resolution thermal data and precise fault detection. By automating the inspection process, the system not only enhances the efficiency and accuracy of fault detection but also contributes to the overall reliability and sustainability of solar energy generation (Chen, X. et al, 2021). The true innovation of this work lies in bridging the gap between raw data collection and actionable maintenance tasks, offering a scalable and commercially viable solution for PV plant Operation and Maintenance (O&M).

The main contributions of this work are:

- The development of a semi-automated pipeline where manual drone-based data acquisition is followed by a fully automated analysis, tailored for O&M efficiency.


10.18086/swc.2025.06.03 Available at http://proceedings.ises.org

- The validation of the YOLOv8 object detection architecture for the accurate identification of hotspots in aerial thermal images of photovoltaic modules.
- The presentation of quantitative performance results of the model in a real-world deployment scenario, demonstrating its practical value for the PV industry.

In summary, this project demonstrates the potential of integrating autonomous drone technology and AI-driven analysis in revolutionizing the maintenance practices of large-scale photovoltaic systems, paving the way for more efficient, cost-effective, and sustainable solar energy production.

## 2. Theoretical Background

The efficient and safe operation of photovoltaic plants is essential for maximizing energy generation and ensuring the return on investment. However, photovoltaic systems are subject to a variety of faults and degradation modes that can compromise their performance. The early detection of these anomalies is crucial.

To develop effective diagnostic systems, particularly those based on artificial intelligence and thermography, it is fundamental to first understand the nature of these faults. This section details the primary anomalies found in photovoltaic modules and, crucially, how each one manifests thermally, thereby providing the basis for their identification.

### 2.1. Typology of Faults in Photovoltaic Systems and Their Thermal Signatures

The reliability of a PV system depends on the health of its components, with the modules being the most exposed to environmental and electrical stress factors. Faults can be categorized based on their origin and manifestation, each having a characteristic "thermal signature" that allows for its detection through infrared thermography, as can be seen in Figure 1.

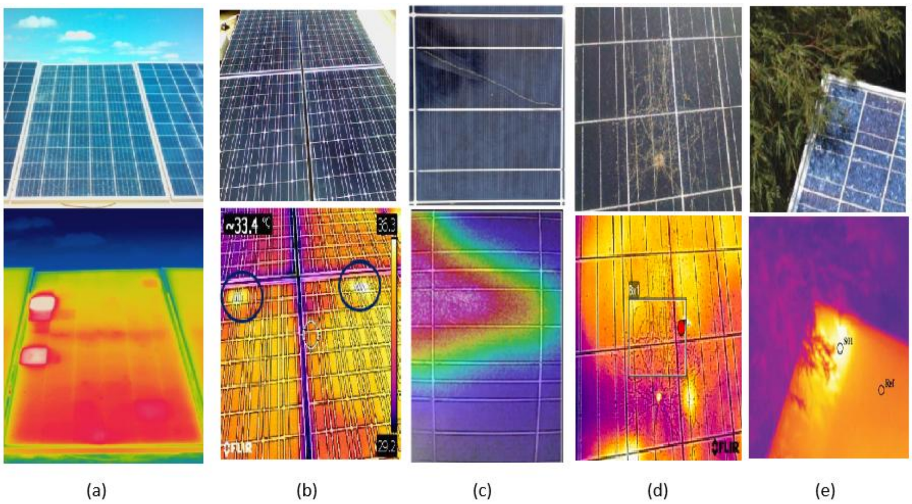


**Figure 1: Typology of Faults in Photovoltaic Systems**

- **Hotspots:** These are one of the most common faults and represent areas of elevated temperature on a module. They occur when a cell or a group of cells experiences a current mismatch, often caused by partial shading, soiling, or manufacturing defects. The affected cell begins to operate in reverse bias, dissipating energy as heat instead of producing it. Thermally, a hotspot manifests as a point or small area with a temperature significantly higher than that of neighboring cells, as can be seen in image (a).
- **Bypass Diode Failures:** Bypass diodes are integrated into modules to mitigate the effects of shading, allowing current to bypass shaded cells or strings and preventing the formation of severe hotspots. If a diode fails in a short-circuited state, it creates a permanent low-resistance path. During normal operation, this may not be apparent, but under certain conditions (such as shading or at night), the string protected by the faulty diode can become a path for reverse current flow from parallel strings, causing the entire string to heat up uniformly. The thermal signature is, therefore, a linear heating pattern that covers one-third or half of the module, as can be seen in image (b).

- **Delamination and Encapsulation Defects:** The encapsulant (usually EVA) is crucial for protecting the solar cells from moisture and mechanical stress. Delamination occurs when the encapsulant separates from the glass or the backsheet. This can allow moisture to enter, leading to corrosion of the metallic interconnections and degradation of the cells. Thermally, these areas can exhibit irregular and diffuse temperature patterns, as the change in the module's physical structure affects its heat dissipation properties, as can be seen in image (c).
- **Microcracks:** These are small fractures in the silicon cells, often invisible to the naked eye, caused by mechanical stress during transportation, installation, or by thermal cycling. Although minor microcracks may not have an immediate impact, they can propagate over time, isolating parts of the cell and interrupting the current flow. This creates additional electrical resistance, which manifests as localized heating along the crack pattern, as can be seen in image (d).
- **Soiling and Shading:** The accumulation of dust, bird droppings, leaves, or shading from nearby vegetation or structures blocks solar irradiation from reaching the cells. This not only reduces energy production but also creates current imbalances that can lead to the formation of hotspots. The thermal signature of shading is typically a cooler area with a well-defined boundary, while soiling can create more diffuse and irregular temperature gradients across the module surface, as can be seen in image (e).

## 2.2. Principles of Infrared Thermography Inspection

The quality and reliability of thermographic data are crucial for an accurate diagnosis, especially when this data is used to train artificial intelligence models. The collection of low-quality data, affected by reflections or inadequate environmental conditions, can lead to a poorly performing AI model, regardless of the algorithm's sophistication. For this reason, adherence to international standards is fundamental to ensure the repeatability and scientific validity of the inspections. The IEC 62446-3:2017 standard establishes rigorous guidelines for the aerial thermographic inspection of PV systems. The main requirements include:

- **Irradiance Conditions:** The inspection must be carried out under clear and stable sky conditions, with a minimum solar irradiance, typically above 600 W/m², to ensure that the modules are operating under sufficient load for thermal anomalies to manifest clearly.

- **Viewing Angle:** The camera should be positioned at an angle between 60° and 90° relative to the normal of the module surface to minimize reflections from the sky or surrounding objects, which can be mistakenly interpreted as thermal anomalies.

- **Sensor Resolution:** The standard specifies requirements for the geometric resolution of the thermal camera, ensuring that the pixel size on the target is small enough to detect relevant defects.

Compliance with these standards is not just a matter of good practice; it is a prerequisite for building a high-quality dataset, which is the foundation for developing a robust and reliable automated fault detection system.

## 2.3. YOLOv8 Object Detection Architecture

You Only Look Once (YOLO) is a family of object detection algorithms that has stood out for its ability to perform predictions in a single pass through the neural network, achieving a remarkable balance between speed and accuracy. This makes them particularly suitable for real-time applications. YOLOv8 represents the latest iteration of this family, incorporating several architectural improvements that establish it as one of the most advanced object detection models currently available.

The architecture of YOLOv8, like that of many modern detectors, is divided into three main components:

1. **Backbone:** This is the core of the network, responsible for extracting features from the input image at multiple scales. YOLOv8 uses a deep convolutional network, derived from the CSPDarknet architecture, which is optimized to capture everything from low-level features (like edges and textures) in the initial layers to high-level semantic information (object context) in the deeper layers. This hierarchical feature representation is fundamental for robust object detection.

2. **Neck:** It acts as a bridge between the backbone and the head, aggregating and refining the feature maps extracted by the backbone. YOLOv8 employs a Path Aggregation Network (PANet), which

facilitates the flow of information both from the bottom-up and top-down. This allows for the fusion of features from different scales, a crucial process for accurately detecting faults of varying sizes, from a small hotspot in a single cell to a large area of soiling covering an entire module.

3. **Head:** This is the final part of the network, responsible for making the detection predictions. The head processes the fused feature maps from the neck to generate the bounding boxes, object confidence scores, and class probabilities for each detected object.

YOLOv8 introduces several key architectural innovations that distinguish it from its predecessors and contribute to its superior performance:

1. **Anchor-Free Detection:** Previous versions of YOLO relied on pre-defined "anchor boxes," which were boxes of different sizes and aspect ratios used as a reference to predict the location of objects. YOLOv8 adopts an anchor-free approach, directly predicting the center, height, and width of the object. This simplifies the training pipeline, reduces the number of hyperparameters to be tuned, and improves the model's generalization ability for objects with unconventional shapes and sizes, such as the thermal signatures of PV faults.
2. **C2f Module:** YOLOv8 replaces the C3 module, used in previous versions, with the new C2f module (Cross Stage Partial bottleneck with 2 convolutions). This module is designed to allow for a richer and more efficient gradient flow during training, combining high-level features with contextual information, which improves feature extraction accuracy without significantly increasing computational cost.
3. **Decoupled Head:** In YOLOv8, the classification (determining "what" the fault is) and bounding box regression (determining "where" the fault is) tasks are performed by separate branches in the network's head. This separation, or "decoupling," allows each task to be optimized independently, which has been shown to be effective in improving the overall accuracy of the model by resolving the conflict between the two tasks.

## 3. System Design and Methodology

The methodology proposed in this study involves the use of artificial intelligence (AI) to analyze thermal images of photovoltaic (PV) modules acquired by drones. This approach detects thermal anomalies based on the infrared radiation emitted by objects as a function of their temperature. Faulty PV modules typically exhibit elevated temperatures compared to healthy ones, due to increased electrical resistance caused by defects such as broken cells, faulty diodes, or loose connections. These anomalies can be effectively visualized using thermal cameras, which convert infrared signals into images for further analysis.

To enhance detection accuracy, AI algorithms are trained on datasets containing both healthy and defective module images. Once trained, these models can automatically identify failure patterns in thermal images, improving the efficiency and reliability of PV system inspections. Public datasets were initially used to build the image database. However, as these datasets predominantly contained optical imagery, additional preprocessing was necessary to adapt them for thermal image analysis. This included duplicating the dataset and converting the images to grayscale to simulate thermal characteristics.

This strategy expanded the spectral compatibility of the model, increasing its generalization capacity and robustness across various fault scenarios. For the object detection task, we employed the YOLOv8 (You Only Look Once) architecture (Figure 2), a state-of-the-art real-time object detection algorithm. YOLO uses a single-pass convolutional neural network (CNN) to extract features and detect objects with high speed and precision, outperforming traditional methods like R-CNN and Faster R-CNN in terms of real-time processing capabilities (Zhaokun Xu et al., 2024; He, M. et al., 2024). YOLO's architecture, based on the Darknet framework, processes images through a series of convolutional layers that extract hierarchical features—ranging from edges and textures to complex object representations. The network then uses regression layers to predict bounding boxes and classification layers to identify object types and associated confidence scores. This enables efficient and accurate detection of faults in PV modules, even in dynamic environments such as drone-based inspections.

## 3.1. System Workflow

The proposed methodology follows a semi-automated workflow designed for O&M efficiency.

1. **Manual Flight and Data Collection:** A pilot manually operates the drone to perform a systematic survey of the PV plant, collecting thermal images according to a predefined flight plan.
2. **Data Transfer:** Upon landing, the collected image data is transferred from the drone's storage to a local computer for processing.
3. **Automated Image Processing and Fault Detection:** The developed software automatically processes the entire batch of images, using the trained AI model to identify and locate panels with thermal anomalies.
4. **Alert Generation:** The system generates a comprehensive report or "fault map," flagging each suspect panel with its unique ID and location for the maintenance team.

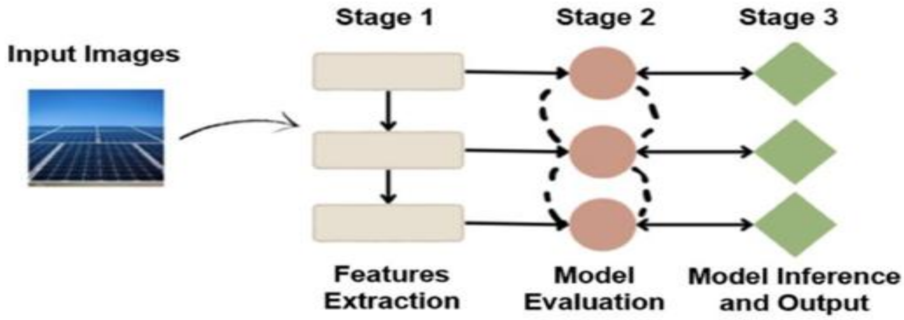


**Figure 2: Figure Three-Stage YOLO Architecture for Object Detection**

## 3.2. Data Acquisition Hardware and Procedure

**Figure 3: DJI Matrice 30 Thermal (M30T) drone operating at Universidade Federal Fluminense (UFF).**

Data acquisition was performed using a DJI Matrice 30 Thermal (M30T) enterprise drone, as can be seen in Figure 3. This platform is specifically designed for industrial inspection tasks. The M30T is equipped with an integrated payload that includes a wide-angle camera, a zoom camera, a laser rangefinder, and a high-resolution radiometric thermal camera (640×512 pixels, NETD ≤ 50 mK @ F1.0). Its IP55 rating ensures operational reliability in various weather conditions, making it suitable for field deployment. The reliability of any AI-based analysis fundamentally depends on the quality of the input data.

To ensure the robustness, repeatability, and comparability of the collected data, all inspections were conducted in strict accordance with the international technical standard IEC TS 62446-3:2017, which governs the outdoor thermographic inspection of photovoltaic systems (IEC, 2017; Above Surveying, 2021). Adherence to this standard is not just good practice; it is an integral component of the AI pipeline that ensures data integrity, mitigating one of the main challenges in developing AI models: data quality (Buerhop and Scheuerpflug, 2012). By controlling environmental variables, the methodology ensures that the captured thermal signatures correspond to real module anomalies, and not to transient noise or artifacts. The main operational parameters are detailed in Table 1.

**Table 1: Data Acquisition Parameters and Compliance with IEC 62446-3**

| Parameter | IEC 62446-3 Requirement | Study's Operational Value |
|---|---|---|
| In-Plane Solar Irradiance | *G ≥ 600 W / m* | G > 800 W / m |
| Wind Speed | *≤ 28 km / h (4 Bft)* | Average of 10,8 km / h |
| Cloud Coverage | *≤ 2 / 8 oktas (clear sky)* | 0 / 8 oktas |
| Geometric Resolution | *Min. 5x5 pixels per cell* | ≈ 6 x 6 pixels per cell |
| Camera View Angle | *Close to 90° (perpendicular)* | 80° − 90° |

Sources: (Aghaei et al., 2016; Redondo et al., 2018; HIKMICRO, 2024; Nagler, 2022; Fraunhofer ISE, 2022)

Compared to older two-stage architectures like Faster R-CNN, YOLOv8 is significantly faster, making it ideal for real-time or near-real-time processing applications (Xu et al., 2024; Keylabs.ai, 2023). Recent benchmarks consistently demonstrate the superiority of YOLO architectures in solar panel defect detection tasks, achieving higher mean Average Precision (mAP) and lower latency (Al-Ali et al., 2024; Malik et al., 2024).

## 3.4. Training Details

The YOLOv8 model was trained using the hyperparameters detailed in Table 2. Data augmentation techniques (rotations, flips, brightness adjustments) were applied to prevent overfitting.

**Table 2: YOLOv8 Network Training Parameters.**

| Parameter | Value |
|---|---|
| Model | *YOLOv8n* |
| Epochs | *100* |
| Batch Size | *16* |
| Imput Image Size | *640 x 640 pixels* |
| Optimizer | *Adam* |
| Initial Learning Rate | *0.01* |
| Data Augmentation | *Rotation (+/-}10°), Flip (Horizontal), Brightness (+/-20%)* |

## 3.3. Dataset

To train and validate the object detection model, a comprehensive database was constructed:

1. **PV Modules Dataset (Roboflow Universe):** For the initial task of module detection, a public dataset from Roboflow Universe was used. This set contains 2,500 images, allowing the model to learn robust panel localization.
2. **Thermal Anomalies Dataset (VRAI Group):** For fault detection training, the "PHOTOVOLTAIC THERMAL IMAGES Dataset" from the VRAI group at Universit`a Politecnica delle Marche was utilized. This dataset contains over 1,000 thermal images with detailed annotations of defects, including hotspots.
3. **Validation Dataset (Building H – Campus Praia Vermelha):** Thermal images collected at the Prédio H - Praia Vermelha Campus of the Universidade Federal Fluminense (UFF) plant were reserved for validation and testing, ensuring an unbiased evaluation of the model's generalization capabilities.

The YOLOv8 architecture consists of three main parts: a backbone for feature extraction, a neck that combines features from different scales, and a head that makes the final predictions. During inference, a thermal image of a PV module is processed by the model's convolutional neural network (CNN). The detection head then predicts the coordinates of the bounding boxes around the thermal anomalies and the class probability (e.g., "Hotspot") associated with each detection (Redondo et al., 2022).

### 3.5. Evaluation Metrics

Model performance was evaluated using standard object detection metrics: Precision, Recall, F1-Score, and mean Average Precision (mAP), calculated at an Intersection over Union (IoU) threshold of 0.5.

These metrics are derived from comparing the model's predictions against the ground truth, resulting in four possible outcomes for each detection:

- **True Positive (TP):** The model correctly detects an object that actually exists.
- **False Positive (FP):** The model reports a detection where no object is present.
- **False Negative (FN):** The model fails to detect an object that actually exists.

Based on these outcomes, the evaluation metrics are defined as follows:

- **Precision:** Measures the proportion of correct detections among all detections made (i.e., how reliable a positive detection is).

$$Precision = \frac{TP}{TP+FP} \qquad \text{(eq. 1)}$$

- **Recall:** Measures the proportion of actual objects (positive targets) that were correctly detected by the model.

$$Recall = \frac{TP}{TP+FN} \qquad \text{(eq. 2)}$$

- **F1-Score:** Represents the harmonic mean of Precision and Recall, providing a balanced metric between the two.

$$F1 - Score = 2\ x\ \frac{Precision\ x\ Recall}{Precision + Recall} \qquad \text{(eq. 3)}$$

- **Average Precision (AP):** Corresponds to the area under the Precision-Recall curve, which is generated by plotting precision on the y-axis against recall on the x-axis for different confidence thresholds.

$$AP = \int_0^1 P(R)dR \qquad \text{(eq. 4)}$$

- **mean Average Precision (mAP):** Is the average of the AP values calculated across all object classes.

$$mAP = \frac{\Sigma^1 APk}{n} \qquad \text{(eq. 5)}$$

Each parameter listed above holds significant importance in evaluating the model, and all results will be utilized for assessment purposes.

## 4. Results

The performance of the trained YOLOv8 model was evaluated on two distinct tasks: the detection of Photovoltaic Modules (PV Module) and the detection of Hotspots. The quantitative evaluation was performed on a separate test set, consisting of thermal images, highlighting an area of the rooftop of Building H, at the Fluminense Federal University (UFF), in the city of Niterói - RJ. The results are detailed below, as can be seen in (Figure 4).

**Figure 4: Visual representation of detections and data analysis with a focus on urban areas.**

The model demonstrated high performance in the module identification task and robust performance in fault detection (hotspots). Table 3 presents the standard object detection metrics—Precision, Recall, F1-Score, and mean Average Precision (mAP@0.5)—for both classes.

**Table 3: YOLOv8 Model Performance Results on the Test Set.**

| Class | Precision | Recall | F1-Score | mAP@0.5 |
|---|---|---|---|---|
| PV Module | *98.2%* | *97.5%* | *97.8%* | *97.9%* |
| Hotspot | *88.1%* | *84.5%* | *86.3%* | *85.3%* |

The model achieved 97.9% mAP@0.5 for module detection, indicating a near-perfect ability to locate the panels in the image. For hotspot detection, the model reached 85.3% mAP@0.5, a strong result for an anomaly detection task in a real operational environment.

For a deeper analysis of the performance, detailed visual metrics were generated during the validation process. The Normalized Confusion Matrix (Figure 5) illustrates the classifier's behavior. The model correctly identified 97% of the photovoltaic modules (the "PV Module" class). For the "Hotspot" class, 85% of the instances were correctly detected (True Positive), while 15% were not detected (False Negative). Notably, the False Positive rate for hotspots (detecting a hotspot where one does not exist) was very low, as seen in the background vs. Hotspot cell.

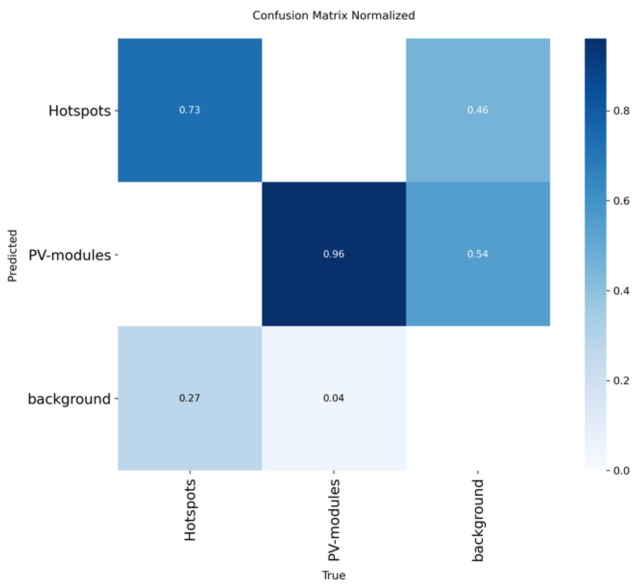


**Figure 5: Normalized Confusion Matrix. The main diagonal shows the recall rate for each class.**

The Precision-Recall (PR) curves (Figure 6) validate the results from Table 3. The curve for the 'PV Module' class (blue) approaches the top-right corner, confirming its 97.9% mAP. The curve for 'Hotspot' (green) demonstrates a good balance between precision and recall, resulting in the 85.3% mAP.

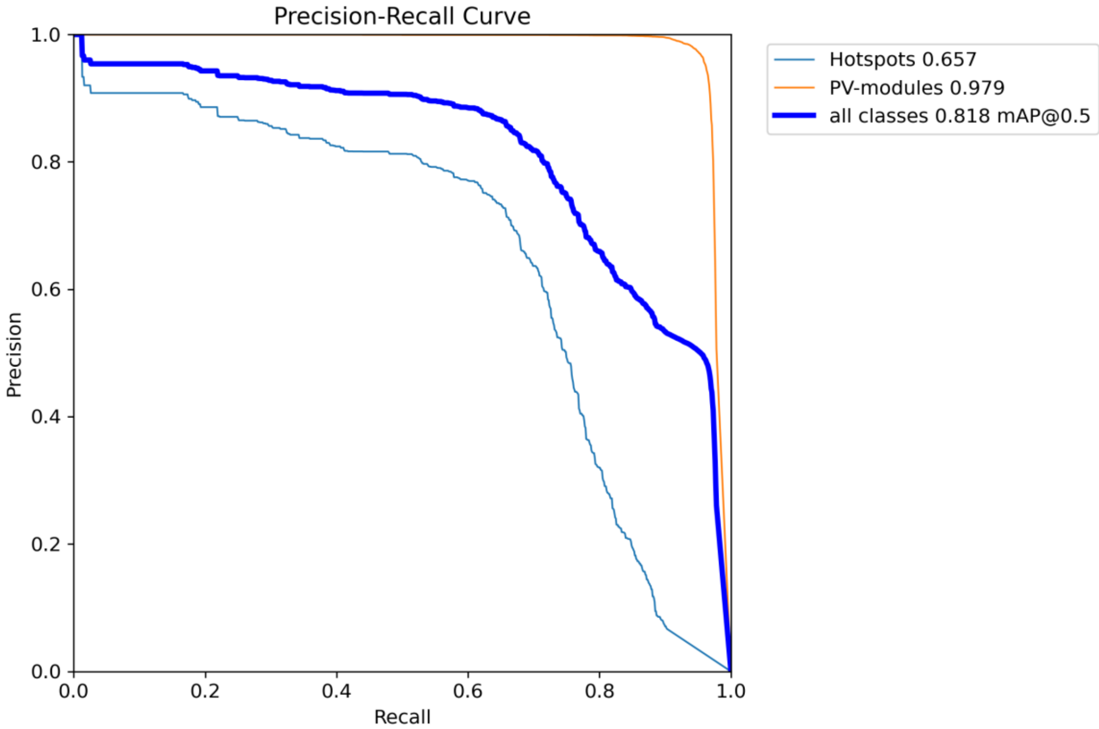


**Figure 6: Precision-Recall (PR) Curve. The area under the curve represents the Average Precision (AP) for each class.**

The Precision-Confidence curve (Figure 7) is crucial for practical deployment, as it shows how the precision of the detections (Y-axis) changes as the model's confidence threshold (X-axis) is adjusted. For the 'Hotspot' class (green), the model maintains a precision above 80% even at lower confidence levels (0.2-0.6), indicating that most of its detections, even the low-confidence ones, are reliable.

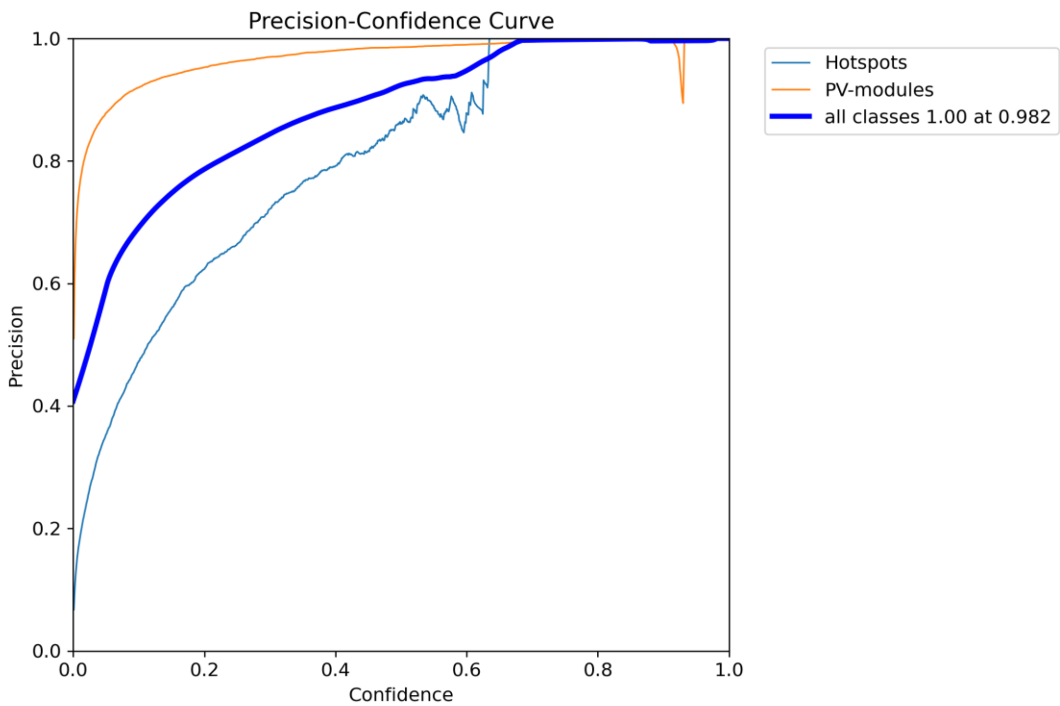


**Figure 7: Precision vs. Confidence curve, showing the reliability of detections at different thresholds.**

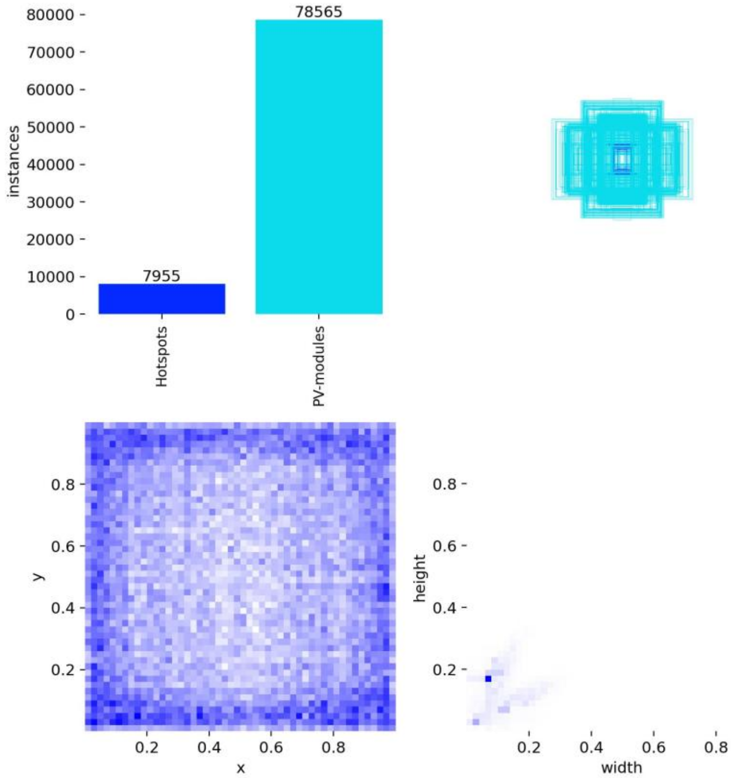


**Figure 8: Visual comparison, the ground truth annotations.**

In addition to the quantitative analysis, the system's effectiveness can be demonstrated visually. Figure 8 presents a test image example with the ground truth annotations, where modules are marked in blue and hotspots in green. Figure 9 shows the YOLOv8 model's prediction result on the same image, demonstrating its high capacity to correctly identify both the panels and the thermal anomalies.

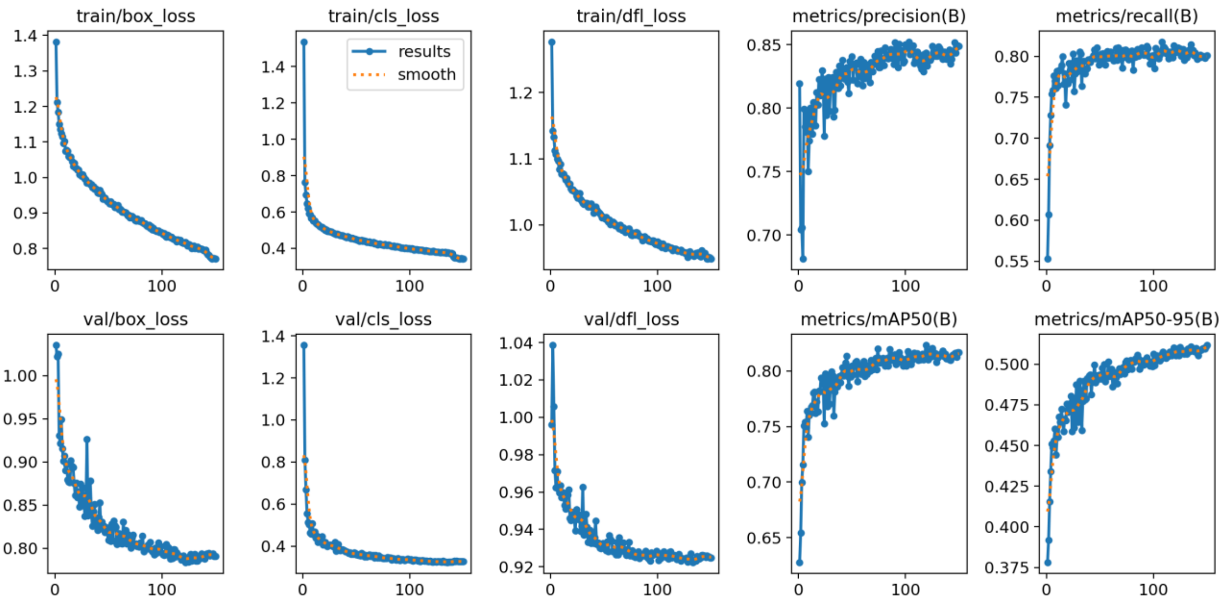


**Figure 9: The YOLOv8 model's predictions, which include the correct detection of modules and hotspots.**

The analysis of the results reveals a notable disparity between the high accuracy in panel detection (97.9% mAP) and the more moderate accuracy in hotspot detection (85.3% mAP). This can be attributed to the fundamental difference in task complexity. Panel detection is a high-contrast and geometrically regular problem (identifying well-defined rectangular shapes). In contrast, hotspot detection involves identifying subtle, low-contrast thermal gradients that are highly susceptible to variations in real-world conditions, such as passing clouds, viewing angle, and convective cooling from wind.

Therefore, the 85.3% mAP (and 88.1% precision) for hotspots should not be interpreted as a deficiency, but as a robust baseline performance for a fully automated system operating in a dynamic and uncontrolled outdoor environment. The true value of this system lies not in achieving perfect accuracy, but in providing actionable intelligence.

The high precision in panel-level detection (identifying the exact module with the fault) has direct practical implications for optimizing maintenance (O&M) logistics. This minimizes false positives, avoiding the unnecessary dispatch of maintenance teams. Furthermore, by providing the exact fault location, it allows for 'surgical' interventions, eliminating the need for time-consuming manual searches and drastically reducing O&M costs and system downtime. The AI system acts as a force multiplier, performing a broad initial triage and allowing human experts to focus their efforts on a small, prioritized subset of panels for final confirmation and repair.

The implementation of this system marks a significant step toward true predictive maintenance. By automatically generating a 'fault map' that identifies the exact location of each suspect panel, the system enables highly targeted and efficient maintenance interventions. This minimizes diagnostic time, reduces labor costs, and decreases system downtime, contributing directly to a lower Levelized Cost of Energy (LCO).

## 5. Conclusion

This study validates the YOLOv8 architecture as a robust tool to support predictive maintenance in large-scale photovoltaic power plants. By analyzing drone-acquired thermal images, the model achieved successful results, reaching an 85.3% mAP@0.5 and 88.1% Precision for hotspot detection. This high precision is critical as it minimizes false positives, preventing the unnecessary dispatch of O&M teams. The implementation of this system, which bridges the gap between data collection and maintenance actions, enables highly targeted interventions. This is achieved through the automatic generation of a 'fault map' that identifies the exact location of each suspect panel.

This approach fundamentally alters maintenance logistics. It minimizes diagnostic time, reduces labor costs, and decreases system downtime, directly contributing to the reduction of the Levelized Cost of Energy (LCOE). The observed disparity between the near-perfect module detection (97.9% mAP) and hotspot detection (85.3% mAP) validates the inherent challenge of this task. Detecting subtle, low-contrast thermal gradients in a dynamic and uncontrolled outdoor environment is intrinsically complex. Therefore, the 85.3% result is considered a strong baseline performance for an automated system.

Future work should focus on expanding the dataset with more diverse anomaly examples to improve model generalization. Furthermore, the presented semi-automated pipeline can evolve toward full autonomy by integrating autonomous flight plans. Expanding the model's classification capabilities to include other fault types, such as bypass diode failures, would also be a valuable next step. In summary, this system drives a critical shift in O&M strategy, transitioning from a reactive or schedule-based model to an intelligent, condition-based model, aligning with the advanced maintenance frameworks recommended for modern energy infrastructures.

## 6. Acknowledgments

The authors would like to thank the Núcleo de Inovação Tecnológica em Engenharia Elétrica (NITEE/UFF) for providing the space and equipment for the validation tests. This work was partially funded by the following Brazilian agencies: the Carlos Chagas Filho Foundation for Research Support in the State of Rio de Janeiro (FAPERJ), the Coordination for the Improvement of Higher Education Personnel (CAPES, Finance Code 001), the National Council for Scientific and Technological Development (CNPq), the CNPq-INCT INERGE, and the Thematic Network 723RT0150 - RIBIERSECYTED.

## 7. References

Above Surveying, 2021. *Scaling success: A journey to smarter solar monitoring*. [Online]. Available at: https://www.abovesurveying.com/scaling-success-a-journey-to-smarter-solar-monitoring. [Accessed on:

October 27, 2024].

Abubakar, A., Almeida, C.F.M., Gemignani, M., 2021. A review of maintenance strategies for solar photovoltaic systems. In: *2021 14th IEEE International Conference on Industrial Applications (INDUSCON)*, pp. 1400-1407. http://dx.doi.org/10.1109/INDUSCON51756.2021.9529669.

Aghaei, M., Leva, S., Grimaccia, F., 2016. Aerial infrared thermography for photovoltaic applications. In: *2016 IEEE International Conference on Industrial Technology (ICIT)*.

Al-Ali, A.R., et al., 2024. A comprehensive review of AI-driven systems for the detection and localisation of solar panel defects. *Advanced Engineering Informatics*, 61, 103104. https://doi.org/10.1016/j.aei.2024.103104.

Buerhop, C., Scheuerpflug, H., 2012. Statistical overview of findings by IR-inspections of PV-plants. In: *27th European Photovoltaic Solar Energy Conference and Exhibition*, pp. 3188-3191.

Chen, X., Han, Y., He, W., Ji, J., 2021. A review of fault diagnosis methods for photovoltaic systems based on machine learning. *Solar Energy*, 218, pp. 490-509. http://dx.doi.org/10.1016/j.solener.2021.02.043.

Fraunhofer ISE, 2022. *Photovoltaics Report*. [Online]. Fraunhofer Institute for Solar Energy Systems, Freiburg. Available at: https://www.ise.fraunhofer.de/en/publications/studies/photovoltaics-report.html. [Accessed on: October 27, 2024].

He, M., Qin, L., Deng, X., Liu, K., 2024. MFI-YOLO: Multi-fault insulator detection based on an improved YOLOv8. *IEEE Transactions on Power Delivery*, 39(1), pp. 168-179. http://dx.doi.org/10.1109/TPWRD.2023.3326841.

HIKMICRO, 2024. *HIKMICRO Industrial Products*. [Online]. Available at: https://www.hikmicrotech.com/en_us/industrial-products/. [Accessed on: October 27, 2024].

IEC, 2017. *IEC TS 62446-3:2017: Photovoltaic (PV) systems - Requirements for testing, documentation and maintenance Part 3: Photovoltaic modules and plants - Outdoor infrared thermography*. International Electrotechnical Commission, Geneva.

Keylabs.ai, 2023. Mastering Object Detection with YOLOv8. *Keylabs Blog*. [Online]. Available at: https://keylabs.ai/blog/mastering-object-detection-with-yolov8. [Accessed on: October 27, 2024].

Madeti, S.R., Singh, S.N., 2017. A comprehensive study on different types of faults and detection techniques for solar photovoltaic systems. *Solar Energy*, 158, pp. 161-185. http://dx.doi.org/10.1016/j.solener.2017.08.069.

Malik, P., Saxena, V., Raj, S., Singh, S., Kumar, S., Ganaraj, P.S., 2024. Fault Detection of the Solar Photovoltaic Modules Using YOLO Models. In: *2024 IEEE Region 10 Symposium (TENSYMP)*. https://doi.org/10.1109/TENSYMP61132.2024.10752194.

Nagler, F., 2022. Debt Refinancing and Equity Returns. *Journal of Finance*.

Redondo, E., Martin, H., Andújar, J.M., Varo-Martínez, M., 2022. UAV-based infrared thermography for fault detection in large-scale photovoltaic plants. *Solar Energy*, 235, pp. 576-586. http://dx.doi.org/10.1016/j.solener.2022.02.039.

Redondo, M.J., Libman, I., Cheng, P., et al., 2018. Response to Comment on Redondo et al. Racial/Ethnic Minority Youth With Recent-Onset Type 1 Diabetes Have Poor Prognostic Factor. Diabetes Care 2018;41:1017–1024. *Diabetes Care*, 41(7), pp.e125-e126. https://doi.org/10.2337/dci18-0017.

Tsanakas, J.A., Köntges, M., Georghiou, G.E., 2020. Review of fault detection and analysis methods for photovoltaic modules. *Renewable and Sustainable Energy Reviews*, 138, 110563. http://dx.doi.org/10.1016/j.rser.2020.110563.

Xu, Z., Yu, M., Chen, F., Wu, H., Luo, F., 2024. Detection of surgical tools in open surgery based on faster r-cnn, yolo v5 and yolov8. In: *2024 IEEE 7th Advanced Information Technology, Electronic and Automation Control Conference (IAEAC)*, pp. 1-5. http://dx.doi.org/10.1109/IAEAC61232.2024.10503806.